Live-fibroblast IR imaging of a cytoprotective PhotoCORM Activated with Visible Light

Zobi, Fabio ; Quaroni, Luca ; Santoro, Giuseppe ; Zlateva, Theodora ; Blacque, Olivier ; Sarafimov, Blagoj ; Schaub, Marcus C ; Bogdanova, Anna Yu

Abstract: Carbon monoxide releasing molecules (CORMs) are an emerging class of pharmaceutical compounds currently evaluated in several preclinical disease models. There is general consensus that the therapeutic effects elicited by the molecules may be directly ascribed to the biological function of the released CO. It remains unclear, however, if cellular internalization of CORMs is a critical event in their therapeutic action. To address the problem of cellular delivery, we have devised a general strategy which entails conjugation of a CO-releasing molecule (here a photoactivated CORM) to the 5'-OH ribose group of vitamin B12. Cyanocobalamin (B12) functions as the biocompatible water-soluble scaffold which actively transports the CORM against a concentration gradient into the cells. The uptake and cellular distribution of this B12-photoCORM conjugate is demonstrated via synchrotron FTIR spectromicroscopy measurements on living cells. Intracellular photoinduced CO release prevents fibroblasts from dying under conditions of hypoxia and metabolic depletion, conditions that may occur in vivo during insufficient blood supply to oxygen-sensitive tissues such as the heart or brain.

DOI: https://doi.org/10.1021/jm400527k

Live-Fibroblast IR Imaging of a Cytoprotective PhotoCORM Activated with Visible Light

Fabio Zobi,*[a] Luca Quaroni,*[b] Giuseppe Santoro,[a] Theodora Zlateva,[c] Olivier Blacque,[a] Blagoj Sarafimov,[b] Marcus C. Schaub [d] and Anna Yu. Bogdanova [e]

Carbon monoxide releasing molecules (CORMs) are an emerging class of pharmaceutical compounds currently evaluated in several preclinical disease models. There is general consensus that the therapeutic effects elicited by the molecules may be directly ascribed to the biological function of the released CO. It remains unclear, however, if cellular internalization of CORMs is a critical event in their therapeutic action. To address the problem of cellular delivery, we have devised a general strategy which entails conjugation of a CO-releasing molecule (here a photo-activated CORM) to the 5'-OH ribose group of vitamin B12. Cyanocobalamin (B_{12}) functions as the biocompatible water soluble scaffold which actively transports the CORM against a concentration gradient into the cells. The uptake and cellular distribution of this B_{12}-photoCORM conjugate is demonstrated via synchrotron FTIR spectromicroscopy measurements on living cells. Intracellualr photo-induced CO release prevents fibroblasts from dying under conditions of hypoxia and metabolic depletion, conditions that may occur in vivo during insufficient blood supply to oxygen-sensitive tissues like heart or brain.

[a] *Institute of Inorganic Chemistry, University of Zürich, Winterthurerstrasse 190, CH-8057 Zürich, Switzerland. Fax: (+41) 044 635 6802; Tel: (+41) 044 635 4623; E-mail: fzobi@aci.uzh.ch*

[b] *Paul Scherrer Institute, Swiss Light Source, CH-5232 Villigen, Switzerland. E-mail: Luca.Quaroni@psi.ch*

[c] *Gipf-Oberfrick, CH-5073, Switzerland. E-mail: theodorazlateva@yahoo.com*

[d] *Institute of Pharmacology and Toxicology, University of Zürich, Winterthurerstrasse 190, CH-8057 Zürich, Switzerland. E-mail: schaub@pharma.uzh.ch*

[e] *Institute of Veterinary Physiology, University of Zürich, Winterthurerstrasse 260, CH-8057 Zürich, Switzerland. E-mail: annab@access.uzh.ch*

Introduction

Despite its reputation as a noxious gas, carbon monoxide (CO) has been recognized in recent years as playing a crucial role as a gasotransmitter.[1] Endogenously, following heme degradation by inducible heme oxygenase-1 and constitutive heme oxygenase-2, CO exerts vasodilatory, antinflammatory and anti-apoptotic effects[2] When exogenously applied, the diatomic molecule mediates therapeutic results in different pathologies including cancer, neurodegeneration, hypertension, heart diseases, liver dysfunction, inflammation and infections.[3] The impact of CO in physiology and medicine has prompted several researchers to develop carbon monoxide releasing molecules (CORMs) as an alternative to the administration of the gas. To date the majority of CORMs are transition metal (TM) carbonyl complexes which under different stimuli are able to deliver CO to diseased or inflamed tissues in order to initiate and promote therapeutic effects at the site of disease. CO release in these molecules may be triggered by different strategies which include simple CO dissociation [4-6], redox or ligand exchange mediated processes [7-12], enzymatic triggering [13, 14] or the use of electromagnetic radiation.[15-17]

In general, at present, CORMs are not designed to target a specific receptor or intracellular target and their potential utility is credited to their fundamental ability to liberate CO. In some instance, however, cellular internalization might be fundamental for CORM activity. Robert Poole and his team have shown, e.g., that the bactericidal effects of CORM-3 result from its cellular uptake.[18-21] While solutions of CO gas also impair bacterial growth, they do not match the effectiveness of the CO releasing molecule. In this case the pronounced bactericidal effects of CORM-3 are ascribed to the ability of the molecule to specifically deliver intracellular CO to heme-containing oxidase(s) and to facilitate the electrogenic transmembrane movement of K+ (or Na+) ions.[22]

Within the CORM field we started to develop CO releasing molecules conjugated to biocompatible scaffolds,[23-25] with a focus on vitamin B_{12}, and we have recently introduced a cyanocobalamin (B_{12}) Re-based CORM coordinated to the axial cyano group of the vitamin (B_{12}-ReCORM-**2** in chart 1).[7] The molecule shows cytoprotective effects on an ischemia-reperfusion injury model of neonatal rat cardiomyocytes (NRCs) but atomic absorption spectroscopy (AAS) measurements indicated no cellular uptake of the molecule.[7, 26] We believe there are two possible explanations for this observation. On one hand it is possible that the CO-releasing profile of B_{12}-ReCORM-**2** ($t_{½}$ of CO release = 20-30 min depending on conditions) does not allow sufficient time for the intracellular accumulation of the molecule. On the other hand, if cellular uptake of the cyanocobalamin CORM conjugate is a B_{12}-mediated process, it is possible that the vitamin is internalized following dissociation of the inorganic CORM unit. We are not aware of any studies dealing with the mechanism of vitamin B_{12} uptake in NRCs. However, in mice, cellular B_{12} uptake is mediated by transcobalamin (TC) transporters with features resembling the human homologues.[27]

Analysis of the structure of human transcobalamin II (TCII) in complex with B_{12} indicates that vitamin docking follows replacement of the cyanide ligand on the cobalt centre with the aromatic imidazole group of a histidine located within the transporter binding pocket.[28] It is thus reasonable to assume that B_{12}-ReCORM-**2** is not internalized in NRCs due to the replacement of the cyanide ligand and, consequently, of the entire Re-based CORM complex. Thus, in order to develop cobalamin scaffolds capable of intracellular delivery of appended CORMs, we have explored a new synthetic method, which entails the synthesis of B_{12} CORM conjugates via activation of the 5'-OH ribose group of the vitamin (see scheme 1).[29] The 5'-OH ribose group of the vitamin was selected because it has been shown to be the only

functional group exposed to the exterior aqueous environment when vitamin B_{12} is docked into TCII.[28] This functional group should then provide the handle for the intracellular delivery of different appended CORMs via this general approach.

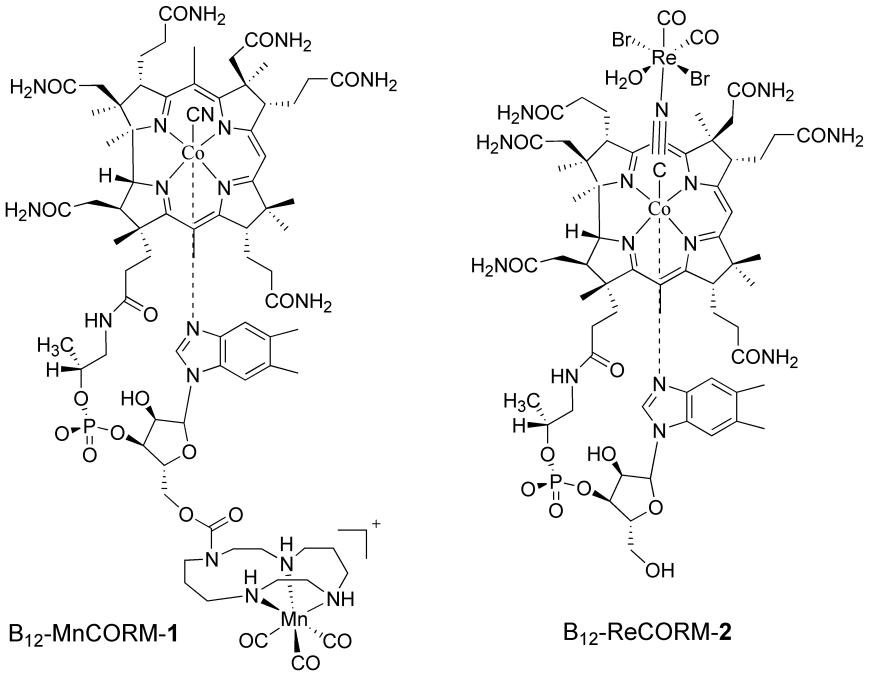

Chart 1. Structures of B_{12}-MnCORM-**1** (left) and of B_{12}-ReCORM-**2**.

Herein we present a novel B_{12}-conjugated photo-activated CO-releasing molecule (B_{12}-MnCORM-**1** in chart 1) based on the *fac*-$[(CO)_3Mn^{I}(tacd)]^{+}$ complex (where tacd = 1,4,8,11-tetraazacyclotetradecane) appended on the ribose sugar moiety of the vitamin via the strategy decribed above. Live 3T3 fibroblast cellular uptake of the molecule was investigated via synchrotron FTIR spectromicroscopy measurements and compared to that of B_{12}-ReCORM-**2**. It is shown that B_{12}-MnCORM-**1** but not B_{12}-ReCORM-**2** is internalized in 3T3 fibroblasts. Furthermore, the intracelluar photo-induced CO release of B_{12}-MnCORM-**1** can be initiated with light of frequency in the visible region of the spectrum. Indeed liquid IR experiments and myoglobin assay studies indicate that CO loss may be promoted either via irradiation with a

LED system (maximum emission centered at 470 nm) or with a green Ar laser (formal highest exciting emission at 496.5 nm). The potential pharmacological value of the molecule is biologically demonstrated by its cytoprotective effect on a cell culture model of 3T3 fribroblasts. Treatment with light activated B_{12}-MnCORM-**1** prevents fibroblasts from dying under conditions of hypoxia and metabolic depletion , conditions as may occur in vivo during insufficient blood supply to oxygen-sensitive tissues like heart or brain. Finally, in our continuing effort to establish a general taxonomy for bioconjugated CORM species, we adopt here for the photoCORM presented (i.e. B_{12}-MnCORM-**1**) the previously proposed nomenclature of the type: X-MCORM-#; where X = carrier biomolecule (here B_{12}); M = transition metal (here Mn); CORM explicitly denotes the function; and # = associated numeric value to differentiate the molecules.

Results and Discussion

Synthesis and Characterization

PhotoCORM B_{12}-MnCORM-**1** was prepared in moderate yield in two steps from the reaction of the cyanocobalamin ligand **1** and the $[Mn^{I}Br(CO)_5]$ complex (see Scheme 1). Compound **1** was first prepared via CDT activation of the 5´-OH group of the vitamin followed by reaction with 1,4,8,11-tetraazacyclotetradecane (tacd). The ligand was obtained in good yield following HPLC purification. HPLC-MS traces recorded during the reaction revealed quantitative activation of B_{12} and the formation of two products in in a 3:1 ratio. The mass of the two species had values of *m/z* = 1582.2 and *m/z* = 2964.2 corresponding, respectively, to **1** and to a B_{12} dimer bridged by a single tacd (Scheme 1). B_{12}-MnCORM-**1** was then obtained via reacting **1** with $[Mn^{I}Br(CO)_5]$ in a methanol solution. Coordination of the pentacarbonyl complex to the pending tacd unit was carried out at room temperature in order to avoid a possible interaction of Mn with the cyano group of B_{12} and subsequent formation of a Co-CN-Mn adduct. The IR spectrum of B_{12}-MnCORM-**1** showed a single ν_{CN} band at 2134 cm^{-1}, at the same frequency of the corresponding stretching vibration of free B_{12}. The absence of the characteristic shift to higher frequency of the ν_{CN} band (by ca. 50 cm^{-1}), typical of Co-CN-TM adducts of bridging cyanides [30-32] (where TM = transition metal), is in agreement with the proposed structure of B_{12}-MnCORM-**1**. Alongside the ν_{CN} band at 2134 cm^{-1} the IR spectrum of the photoCORM showed two ν_{CO} stretching frequencies at 2026 and 1922 cm^{-1} which are characteristic of *fac*-$[Mn^{I}(CO)_3L_3]^n$ species.[25, 33]

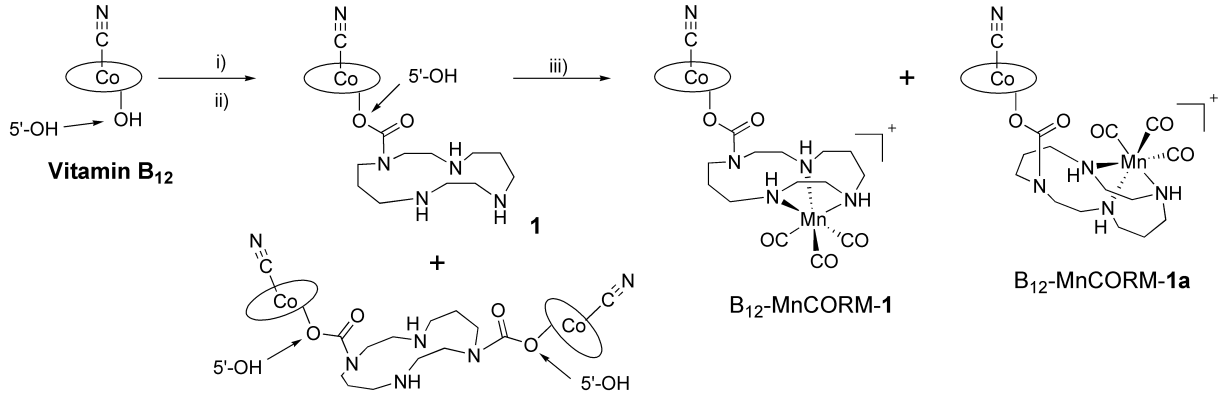

Scheme 1. Synthesis of photoCORM B_{12}-MnCORM-**1**. Reagents and conditions: i) CDT, DMSO, 12 h, RT; ii) tacd, DMSO, 24 h, RT; iii) $[Mn^{I}Br(CO)_5]$, methanol, 24 h, RT.

HPLC-MS traces recorded during the formation of B_{12}-MnCORM-**1** showed the formation of a second product (B_{12}-MnCORM-**1a** in scheme 1) in a relative 4:1 ratio. In our systems the two peaks were separated by ca. 1 min. Both species showed the same mass at *m/z* = 1720.8 and with the same isotope pattern expected for the desired product. We initially speculated that the difference in retention times might be due to different counter anions (i.e. Br^- from $[Mn^{I}Br(CO)_5]$ and $CF_3CO_2^-$ in HPLC solvents) neutralizing the cationic photoCORM, but this conclusion was dismissed considering that our HPLC system is not able to discriminate such difference with an accuracy of 1 min. The two peaks were then separately collected, allowed to equilibrate in solution for 30 min and then reanalyzed. We found no evidence of an equilibrium between the two species. When pooled together into a single vial the HPLC trace of the resulting solution revealed the same separation observed in the crude mixture. This evidence pointed to two structurally different complexes. Attempts to obtain single crystals of the two species suitable for X-

ray diffraction studies proved unsuccessful. However, in order to obtain insights into the structure of the adducts, calculations at the density functional level of theory were performed.

The gas phase optimized structures of B_{12}-MnCORM-**1** and B_{12}-MnCORM-**1a** are shown in figure 1. For the major product (i.e. B_{12}-MnCORM-**1**), DFT calculations placed the $[(tacd)Mn^{I}(CO)_3]^+$ unit directly under the PO_4^- group of the phosphodiester linker of the vitamin loop. The complex is stabilized in this position by hydrogen-bonding interactions between two amino NH protons of the tacd ligand and the phosphate oxygen atom labelled O1 in figure 1 (average O··H = 2.03Å) . In order to intercept other possible local structural minima, calculations were attempted with different starting geometries, where the hydrogen-bonding interactions were distrupted by rotating the $[(tacd)Mn^{I}(CO)_3]^+$ unit about the amide bond connecting it to B_{12}. In all cases the starting geometries reverted back to the conformation shown in figure 1. It should be mentioned that in an aqueous environment this conformation is unlikely to persist. Solvent molecules are expected to strongly interact with the phosphate group therby allowing the $[(tacd)Mn^{I}(CO)_3]^+$ complex to rotate about the amide bond with a relatively low activation barrier.

The DFT geometry of B_{12}-MnCORM-**1** was then taken as the starting point for the structural optimization B_{12}-MnCORM-**1a**. The *fac*-$[Mn^{I}(CO)_3]^+$ core was first removed and then reintroduced with the carbonyl ligands pointing towards the the PO_4^- group. As expected, this arrangement imposed a severe steric strain on the geometry which was relieved in the calculations by unwinding the $[(tacd)Mn^{I}(CO)_3]^+$ complex away from the vitamin. Structural parametes of the carrier vitamin and of the complex were found similar in both species with the most notable difference being an increase in the interatomic Mn-P

distance by more than 2 Å in B_{12}-MnCORM-**1a**. Finally this latter geometry was found to be only 0.4 kcal higher in energy than that of B_{12}-MnCORM-**1**.

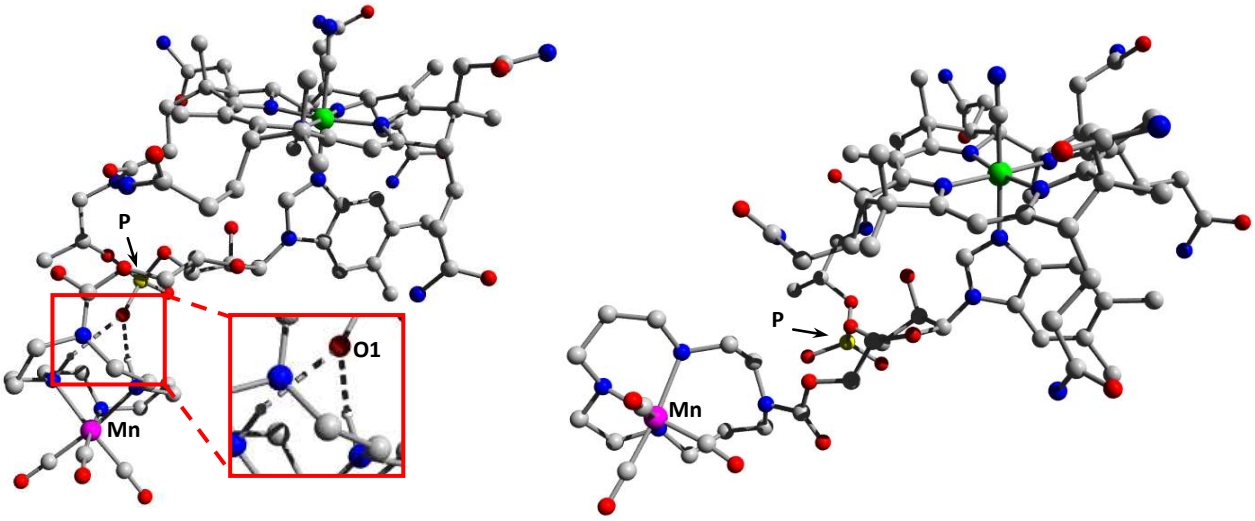

Figure 1. DFT calculated structures of B_{12}-MnCORM-**1** (left) and B_{12}-MnCORM-**1a**.

B_{12}-MnCORM-**1** and -**1a** are soluble in water. As expected, owing to the chemistry of the *fac*-$[Mn^{I}(CO)_3]^+$ core, the compounds are stable in solution and as a solid if kept in the dark. The UV-visible spectra of B_{12}-MnCORM-**1** and -**1a** are virtually identical to that of native B_{12} with the exception of a slightly pronounced absorption in the soret region attributed to the presence of the *fac*-$[(tacd)Mn^{I}(CO)_3]^+$ (**2**) complex (*vide infra*). Over a period of 24h, no change was observed in the spectrum of a solution of the photoCORMs kept in the dark at 50 ºC.

CO Releasing Properties of B_{12}-MnCORM-1.

The photo-induced carbon monoxide releasing properties of B_{12}-MnCORM-**1** were evaluated by liquid IR spectroscopy and the myoglobin assay (figure 2).[21, 25] Two sets of experiments were performed using two different light sources. The UV-vis spectrum of the *fac*-[(tacd)$Mn^{I}(CO)_3$]Br complex (**2**) was first determined in order to select the appropraiate irradiation wavelength. In an unbuffered aqueous solution **2** shows a maximum absorption centered at 388 nm. DFT calculations indicated that this absorption is composed of several excitations of which the seven major ones involve HOMO (HOMO-3 to HOMO) to LUMO (LUMO to LUMO+9) transitions between orbitals mainly of metal character. In oder to promote CO loss from the photoCORM, initially a LED system (blue visible light with maximum emission at 470 nm) was employed. The emission profile of this LED systems shows a significant overlap with the absorption band of **2** (figure 2A). In a second instalment, experiments were performed using a green Ar laser. In this case, laser emissions with fequencies higher than 658.9 THz were eliminated via the use of a 455 nm optical cutoff filter positioned between the laser source and the sample. Analysis of the superiposition of the laser emission lines and the absorption spectrum of **2** reveals an overlap of six distinct excitation wavelengths ranging from 457.9 to 496.5 nm (see figure 2A)

The behaviour and CO releasing properties of B_{12}-MnCORM-**1** were first studied in a methanol solution by IR spectroscopy using an *in situ* IR deep probe. In solution the complex shows two characteristic ν_{CO} stretching frequencies at 2031 and 1930 cm^{-1}. In the dark no change was observed over a 12h period. Upon exposure to the LED source the two peaks began to decrease steadily, disappering after 3h of illumination (figure 2B). No intermediates were observed during the photolysis. When the green Ar laser was used a

similar behaviour was observed but with much slower kinetics of CO release.

Under experimental conditions of a typical myoglobin assay, irradiation of B_{12}-MnCORM-**1** with the LED source elicited the spectral changes associated with CO release. This was determined by following the absorption spectra of the Q band of deoxy-myoglobin (deoxy-Mb) at 551 nm as it converted to carbon monoxide myoglobin (MbCO) with two maximal absorption peaks at 540 and 578, respectively (figure 2C). The conversion proceeded cleanly with six isosbestic points clearly visible in the spectrum. When experiments were performed under conditions of a limiting amount of B_{12}-MnCORM-**1**, taking into account the molar extinction coefficient of MbCO, it was found that approximately 3 mol of CO were released per mole of the corresponding complex within 1 hour. To confirm the identy of the resulting species, following photo-induced carbon monoxide release, samples of the photoCORM were analyzed by HPLC-MS. It was determined that the only vitamin B_{12} species present in solution was the free ligand **1**, indicating complete dissociation of the *fac*-$[Mn^{I}(CO)_3]^+$ core.

Under similar conditions, the spectrum of the conversion of deoxy-Mb to MbCO promoted by irradiation of B_{12}-MnCORM-**1** showed disticly different features when the Ar laser was used (figure 2D). Qualitatively the spectral changes confirm CO release by the photoCORM and formation of MbCO. However, after prolonged exposure to the electromagnetic radiation, photolysis of the Mb-bound CO was also observed. This process was evidenced by the appearance after 2h of irradiation, of a small peak at 640 nm, characteristic of metmyoglobin (MetMb).

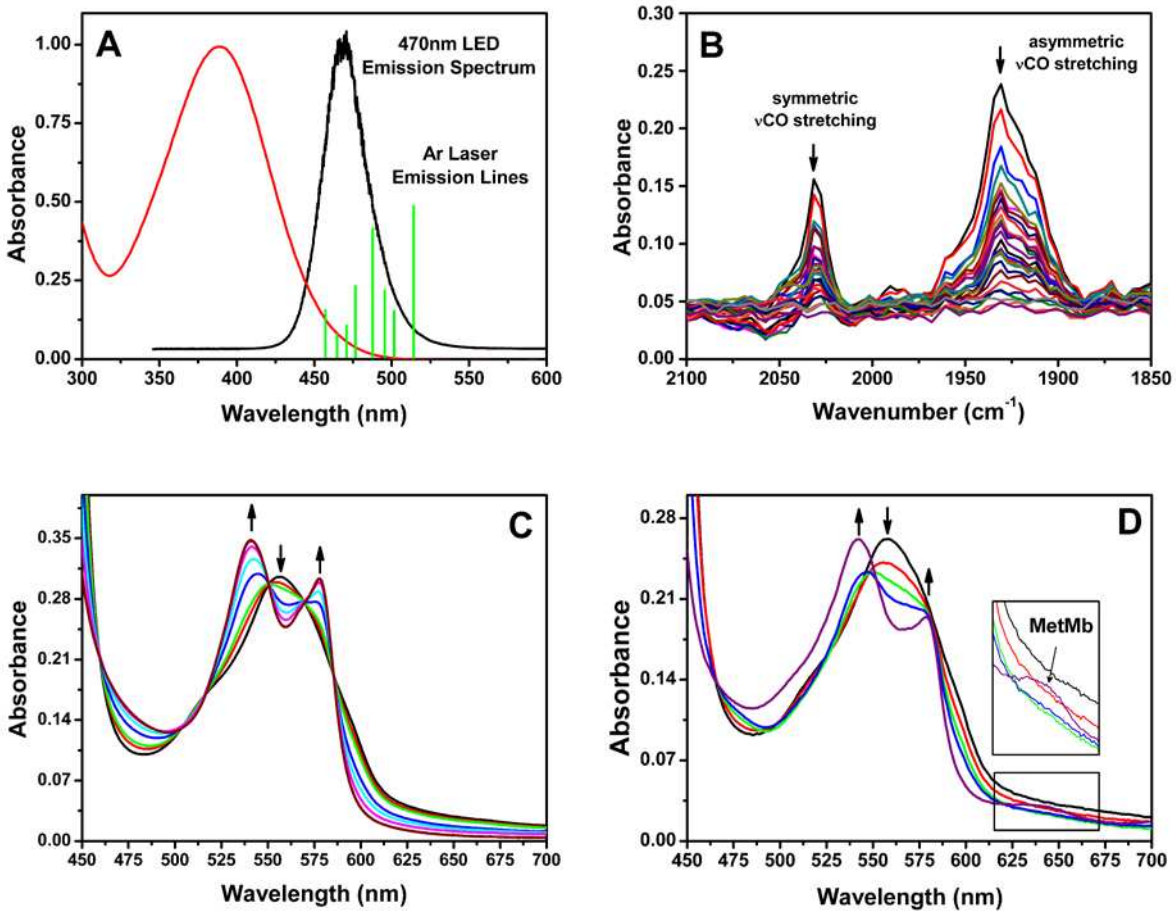

Figure 2. A: UV-visible spectrum of 2 in an unbuffered aqueous solution (red); emission spectrum of LED source (black); relative intensity of green Ar laser emission lines (green). B: changes in the liquid IR spectrum of a 4 mM solution of B_{12}-MnCORM-1 exposed to LED source. C: conversion of deoxy-myoglobin (deoxy-Mb) to carbon monoxide myoglobin (MbCO) by B_{12}-MnCORM-1 exposed to LED source (20 μM Mb and photoCORM, 25°C, 0.1 M phosphate buffer pH 7.4, spectra intervals = 5min). D: conversion of deoxy-myoglobin (Mb) to carbon monoxide myoglobin (MbCO) by B_{12}-MnCORM-1 exposed to green Ar laser (20 μM Mb and 60 μM photoCORM, 25°C, 0.1 M phosphate buffer pH 7.4, spectra intervals = 30min). Insert shows the formation of metmyoglobin (MetMb) after prolonged exposure to the light source.

Fibroblast Uptake and Localization of B_{12}-MnCORM-1 and B_{12}-ReCORM-2.

We studied the interaction of B_{12}-MnCORM-**1** and B_{12}-ReCORM-**2** with the 3T3 NIH line as a cellular model system and used Synchrotron IR Spectromicroscopy to follow its real time uptake and subcellular localization. IR spectroscopy is capable of detecting molecular chromophores, without any need of exogenous labelling, and to provide structural information about the same.[34] When implemented as a spectromicroscopy technique, it allows us to monitor molecular distribution and structure in microscopic samples.[35, 36] The use of a synchrotron light source further enhances the performance of the technique by improving the signal-to-noise ratio (SNR) when measuring at diffraction limited spatial resolution.[37] In measuring cellular spectra, IR spectromicroscopy records spectral contributions from all molecules in the sample. The complexity of cellular composition is reflected in the complexity of the resulting IR spectra.[38, 39] However, the carbonyl stretching vibrations appear in a spectral region, between 1800 cm^{-1} and 2100 cm^{-1}, which is clear of other absorptions from the most abundant cellular components.

3T3 cells were grown as an adherent phenotype on CaF_2 optical slides, transparent to IR radiation in the spectral range above 950 cm^{-1}. The cells were washed with medium containing 1mM of either B_{12}-MnCORM-**1** or B_{12}-ReCORM-**2** under dim light, enclosed in a thermostatic holder set at 37 °C and moved to the IR microscope for inspection. A single cell was selected under dim light and its IR absorption spectrum recorded as a function of time. Difference spectra are calculated by subtracting the first spectrum of the sequence from the following ones. Positive bands correspond to the accumulation or formation of molecules that occurs in the probed volume, inside or in the proximity of the cell, while negative bands correspond to the expulsion or decomposition of molecules in the same volume.

When 3T3 fibroblasts were treated with a solution of B_{12}-ReCORM-**2** no cellular accumulation was observed over a period of several hours of incubation. However, when the same cells were incubated with B_{12}-MnCORM-**1** difference IR spectra showed slowly evolving spectroscopic changes. The spectra are shown in figure 3. Most changes correspond to variations of absorbance in the range 10^{-4} - 10^{-3} au per minute, above the level of noise. It is to be noted that the use of a bright synchrotron source of IR light has been critical in obtaining sufficient signal-to-noise in the measurement of the weak changes associated with real time uptake in Figure 3. The spectral region between 1800 cm^{-1} and 2100 cm^{-1}, where carbonyl absorptions are expected, displays a series of positive and negative variations. Only two bands are expected for the E and A_1 transitions of a facial tri-carbonyl complex, indicating that chromophores other than the CORMs are contributing to the variations.

We used a two-dimensional correlation spectroscopic (2D-COS) analysis to simplify the picture by identifying sets of bands attributable to specific chromophores. This approach has been described in detail elsewhere.[40] 2D-COS was introduced by Noda as a tool to analyze complex spectral patterns that evolve as a function of a parameter.[41] The analysis provides a quantitative assessment of the phase relationship existing between the evolving bands of chromophores and allows its parameterization. In applications to complex biological systems it has been shown that the analysis allows the identification of bands arising from the same molecular chromophore.[40, 42] Additional features that make 2D-COS useful for the analysis of cellular spectral patterns are the improved spectral resolution and the possibility to extract weak bands evolving on a noisy background.[40, 43]

The results of a 2D-COS analysis of the spectral changes from figure 3 are shown in

figure 4, with the 2D synchronous (A) and asynchronous (B) correlation plots shown separately. Bands from the same chromophore display synchronous correlation, change perfectly in phase and give rise to matching positive off-diagonal peaks in the synchronous plot. For the same reason, bands arising from the same chromophore do not display any off-diagonal peaks in the asynchronous plot. The pair-wise analysis of peak correlations allows the clustering of peaks arising from the same chromophore.

Applying this analysis to the plots in figure 4 shows that six different molecular species are responsible for the spectral variations of figure 3. The largest ensemble of peaks is assigned to water vapor, arising from small changes in the atmosphere surrounding the sample chamber. An additional ensemble of peaks is dominated by the two peaks at 1931 cm^{-1} and 2027 cm^{-1}, at frequencies characteristic for the E and A_1 transitions of B_{12}-MnCORM-**1**. These peaks are positive, indicating that the concentration of B_{12}-MnCORM-**1** is increasing in the measured volume.

From uptake measurements, it is assumed that the observed concentration increase is localized within the cell or at its surface. Detailed mapping of the chromophore, as described later, is necessary to clarify the cellular distribution of the compound. By using Lambert Beer's Law with absorption coefficients (ε) of 150 $mM^{-1}\mu m^{-1}$ (A_1) and 170 $mM^{-1}\mu m^{-1}$ (E) we can estimate a nominal rate of accumulation of 3 μM/min. This nominal rate is to be interpreted as an averaged concentration change over the volume probed by the beam. This volume includes the medium above and surrounding the cell. The effective concentration inside the cell can be extracted by knowing the ratio of the cell volume to the volume probed by the beam. Although the exact value varies from cell to cell, an approximate value of 0.5 can be estimated, giving a cellular rate of uptake of 6 μM/min.

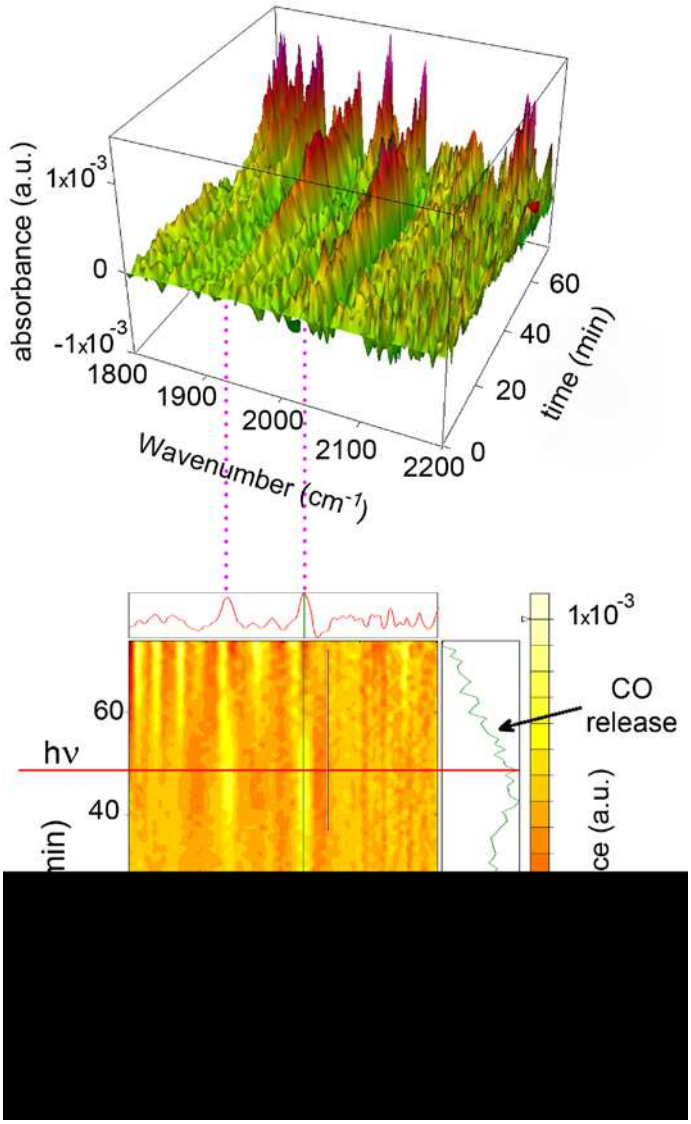

Figure 3. Accumulation and subsequent photolysis of B_{12}-MnCORM-**1** in a single 3T3 fibroblast. Pictures show the time evolution of the IR spectrum of a 3T3 cell incubated with B_{12}-MnCORM-**1** in a 2D (bottom) and a 3D (top) representation. The green line in the frame of the 2D spectrum is a "cross section" along the time direction shown in the plot; the horizontal red line (hv) at ca. 49 min indicates start of illumination by xenon light. a.u. = arbitrary absorbance units. Marked peaks correspond to the E and A1 stretching modes of the *fac*-$[Mn^{I}(CO)_3]^+$ core.

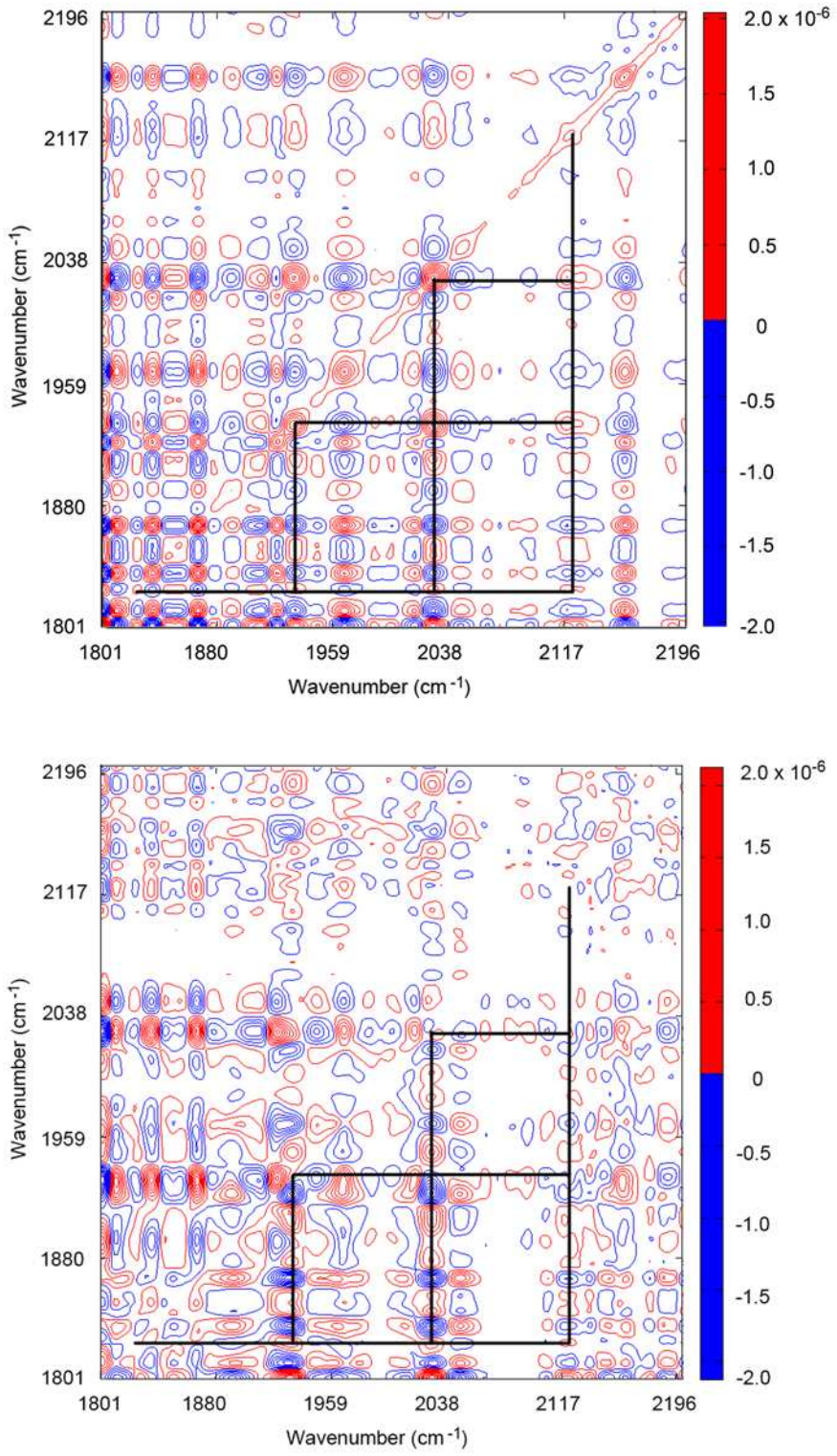

Figure 4. Results of 2D-COS analysis of the spectra reported in figure 3 Top: Synchronous Correlation. Bottom: Asynchronous Correlation.

The cyanide ligand of the corrine complex has an absorption band, corresponding to the stretching of the CN triple bond, at 2132 cm^{-1} in solution. This is a spectral region relatively clear of other molecular absorption bands. Nonetheless, no bands associated to cyanide are seen in the spectra of figure 3. 2D-COS plots allow extracting weak evolving bands from noisy backgrounds, taking advantage of their higher degree of auto correlation relative to noise. Indeed analysis of the synchronous correlation plot reveals the presence of a contribution from a band at 2132 cm^{-1}. The band evolves in phase with the carbonyl bands at 1931 cm^{-1} and 2027 cm^{-1}, although with small off-phase component observed in the asynchronous plot.

After reaching a cellular concentration of 0.24 mM B_{12}-MnCORM-**1**, we exposed the sample to the light of the microscope halogen illuminator, at 75% of total power, while continuously measuring the IR absorption spectrum. Under these conditions the carbonyl bands at 1931 cm^{-1} and 2027 cm^{-1} disappear over the course of ten minutes, in agreement with a photolytic decomposition of B_{12}-MnCORM-**1**.

To obtain information on the localization of B_{12}-MnCORM-**1** within the cell, in separate experiments we performed IR mapping at diffraction limited spatial resolution of a cell after uptake of the compound. A sample of 3T3 cells was exposed to a 1 mM solution of B_{12}-MnCORM-**1** for a few hours, to ensure completion of the uptake process and stabilization of the spectra. A final average concentration of 1.0 - 1.5 mM B_{12}-MnCORM-**1** within cell was achieved. One cell was then selected and mapped by using a 36x (0.5 NA) Schwarzschild objective and a confocal aperture set at 5 x 5 μm^2. Under these conditions, spatial resolution R at 2000 cm^{-1} (λ = 5 μm), according to Rayleigh's criterion,

is R ~ λ = 5 μm. At such concentrations of B_{12}-MnCORM-**1** spectra with a very good signal-to-noise ratio are obtained (see supplementary FigureS6). This allows us to partially resolve the spatial distribution of carbonyl absorptions inside and in the proximity of the cell. An adherent 3T3 cell is about 10-15 μm by 25-30 μm in size, excluding the cellular extensions, with a nucleus about 10-15 μm across, approximately in the center of the extended cell (figure 5). It is therefore possible to resolve the distribution of the carbonyl bands between the inside and outside of the cell and between the cytoplasmatic and nuclear regions. However, resolution is insufficient to resolve smaller organelles.

The maps of figure 5 show that carbonyl bands are present throughout the interior of the cell but much stronger in the central region of the cell, corresponding to the putative location of the nucleus. Caution is necessary in interpreting this observation quantitatively. The topography of an adherent fibroblast cell is characterized by a thicker bulge, corresponding to the nuclear location, surrounded by a much thinner cytoplasmic region that slopes towards the edges of the cells. Therefore, the optical path through the adherent cell is longer in the nuclear region: a molecule with a uniform cellular distribution would still show higher absorbance in the nuclear region. Two conclusions can be extracted from the maps of figure 5. The first one is that the carbonyl bands are clearly located within the cell, thus confirming that uptake has taken place. The second one is that their accumulation is not restricted to the cytoplasm, or a clear gap would appear in the nuclear location.

In order to confirm cellular and nuclear accumulation of B_{12}-MnCORM-**1**, atomic absorption measurements (AAS) were performed on 3T3 fibroblasts incubated with 100

μM the compound for 6h (see experimental section and supporting information). Analysis of the Mn content in whole cells revealed a total intracellular concentration of ca. 10 mM/mg protein of B_{12}-MnCORM-**1**. Partitional analysis of the nuclear and of the cytosolic fractions showed a relative Mn concentration of 0.73:1. By considering estimates of the relative cellular and nuclear volumes of mouse fibroblasts,[44, 45] the above ratio may be as high as 0.8:1, indicating overall a substantial nuclear accumulation of the photoCORM.

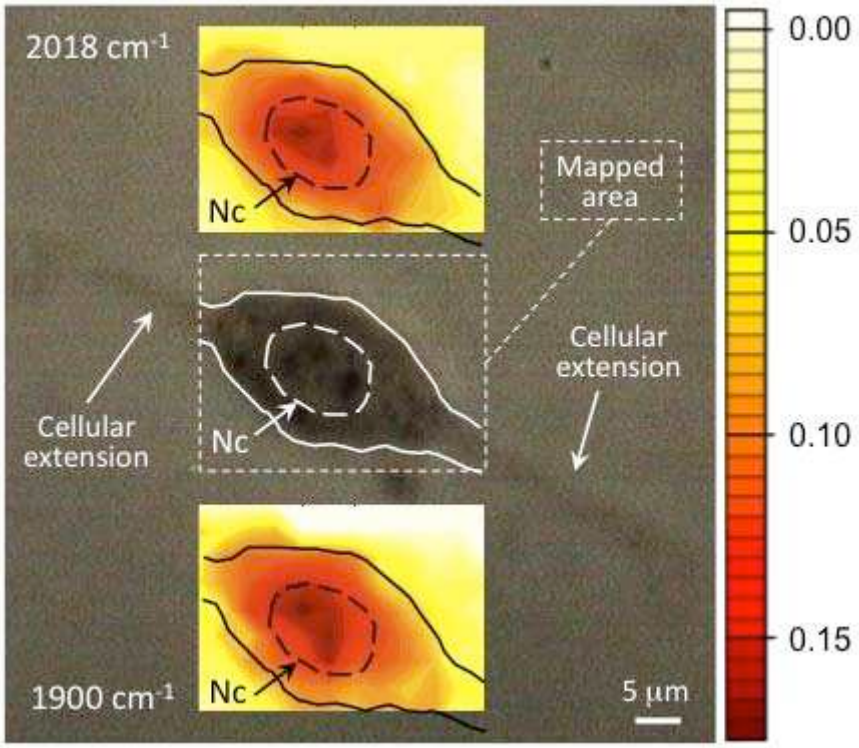

Figure 5. Optical image of a 3T3 fibroblast incubated with B_{12}-MnCORM-**1**. Top and bottom inserts show images reconstructed from integrating the intensities of the carbonyl stretching vibrations at frequencies of 2018 and 1900 cm^{-1} respectively. The scale represents units of integrated band area in an absorbance vs. wavenumber spectrum. Nc = cell nuclear area.

In addition, the maps are consistent with the possibility that a larger amount of carbonyl complex might have accumulated in the nucleus. A nuclear or perinuclear accumulation of metal carbonyl complexes has already been proposed by other authors using a variety of vibrational imaging techniques.[46-48] However, this cannot be confirmed quantitatively without having an exact model of cellular topography to correct for cell thickness effects.

It is notable that the carbonyl bands mapped in figure 5 have different positions than the ones observed during uptake, the former being at 1900 cm^{-1} and 2018 cm^{-1} and the latter being at 1931 cm^{-1} and 2027 cm^{-1}. The difference may be attributed to a variation in the secondary coordination sphere of the metal carbonyl complex reflecting perhaps the transition from lipophilic surroundings (e.g. cellular membrane) to a more hydrophilic environment.

Cytoprotective effects of B_{12}-MnCORM-1 tested on fibroblast cell culture

In contrast to B_{12}-ReCORM-**2** that was not taken up by 3T3 cells, B_{12}-MnCORM-**1** was accumulating within the cells over about one hour's time (figure 3). Judging from the intensity of the carbonyl frequencies characteristic for B_{12}-MnCORM-**1** recorded inside and outside a fibroblast after incubation in 1 mM solution of B_{12}-MnCORM-**1** for a few hours, its intracellular signal intensity was roughly 10 times higher than outside (figure 5). This was estimated to correspond to a final concentration of 1.0 - 1.5 mM B_{12}-MnCORM-**1** within the cell. It looks as if the compound was also taken up by the cell nucleus, although its subcellular repartition cannot be determined unequivocally by present day technology. Nevertheless, the results indicate that B_{12}-MnCORM-**1** is actively transported against a concentration gradient into the cells. In fact, the cellular uptake of vitamin B_{12} has recently been shown to involve a complex transport machinery involving more than 15 gene products.[49] Once inside, CO may be liberated from the compound by photolysis with white light as demonstrated in figure 3. The spectral changes recorded over the cell area caused by CO photolysis are further proving the intracellular localization of B_{12}-MnCORM-**1**.

The cytoprotective properties of B_{12}-MnCORM-**1** were tested on the 3T3 fibroblast cell culture system. 10 minutes after administration of 30 µM B_{12}-MnCORM-**1** half of the culture dishes were exposed to light (xenon lamp at a distance of 10 cm for 15 min) to photolyse CO, while the other half was kept in the dark (see Experimental Section). The results of counting live and dead cells after treating fibroblast cultures with B_{12}-MnCORM-**1** are summarized in figure 6. Treatment of fibroblast cultures with 30 µM B_{12}-MnCORM-**1** displayed no overt cytotoxicity as judged from viable cell numbers and cytochemical morphology. In analogy to the estimate of a cellular uptake rate of around 6 µM per minute in single fibroblasts (see above) in the presence of 1 mM B_{12}-MnCORM-**1** (figures 3 and 5), the concentration of the

compound in the cultured cells exposed to 30 µM B_{12}-MnCORM-**1** may reach 10-20 µM within 10 minutes when illumination started. Thus, in the fibroblast culture experiments the B_{12}-MnCORM-**1** may be present inside and outside the cells. However, during the time course of 48 hours the compound may further accumulate inside the cells with advancing time. Illumination may thus activate B_{12}-MnCORM-**1** inside and outside the cells and the CO released outside will enter cells by permeating through the surface membrane and contribute to the cellular effects.

During the time course experiments, the fibroblasts in culture settled down to the bottom of the dishes. Nuclear staining with Hoechst-33342 yielded the total number of attached cells, while PI stained the fraction of cells destined for death whose surface membrane was lesioned. The lesioned PI-positive cells gradually detached from the bottom of the dishes. This is demonstrated in figure 6A where attached cells under normoxia proliferated with time displaying saturation characteristics leveling between 400 and 500 cells per culture dish. Under hypoxia and metabolic depletion cell numbers followed a similar course but after 26 hours they began to decline significantly. On the other hand, total numbers of cells attached to the substratum in cultures under hypoxia and treatment with light-activated B_{12}-MnCORM-**1** remained relatively low, oscillating between 100 and 200. At 41 hours statistic t-values of total cell numbers for normoxic controls versus both hypoxic with and without B_{12}-MnCORM-**1**-treatment reached levels which corresponded to $p<0.01$ (figure 6A asterisk). Under hypoxia the fraction of PI-positive dead cells increased from 26 hours till the end of the experiments (figure 6C), thus mirroring the decline of the numbers of attached cells under hypoxia. Significances of dead cell fractions between hypoxic cultures versus normoxic and hypoxic cultures treated with B_{12}-MnCORM-**1** could not be established, because the dead cell fractions were quite variable. This might be due to the variable number of cells that were

detached from the substratum. Consequently, the numbers of "dead cells still attached" may represent a variable underestimate of the actual amounts of dead cells.

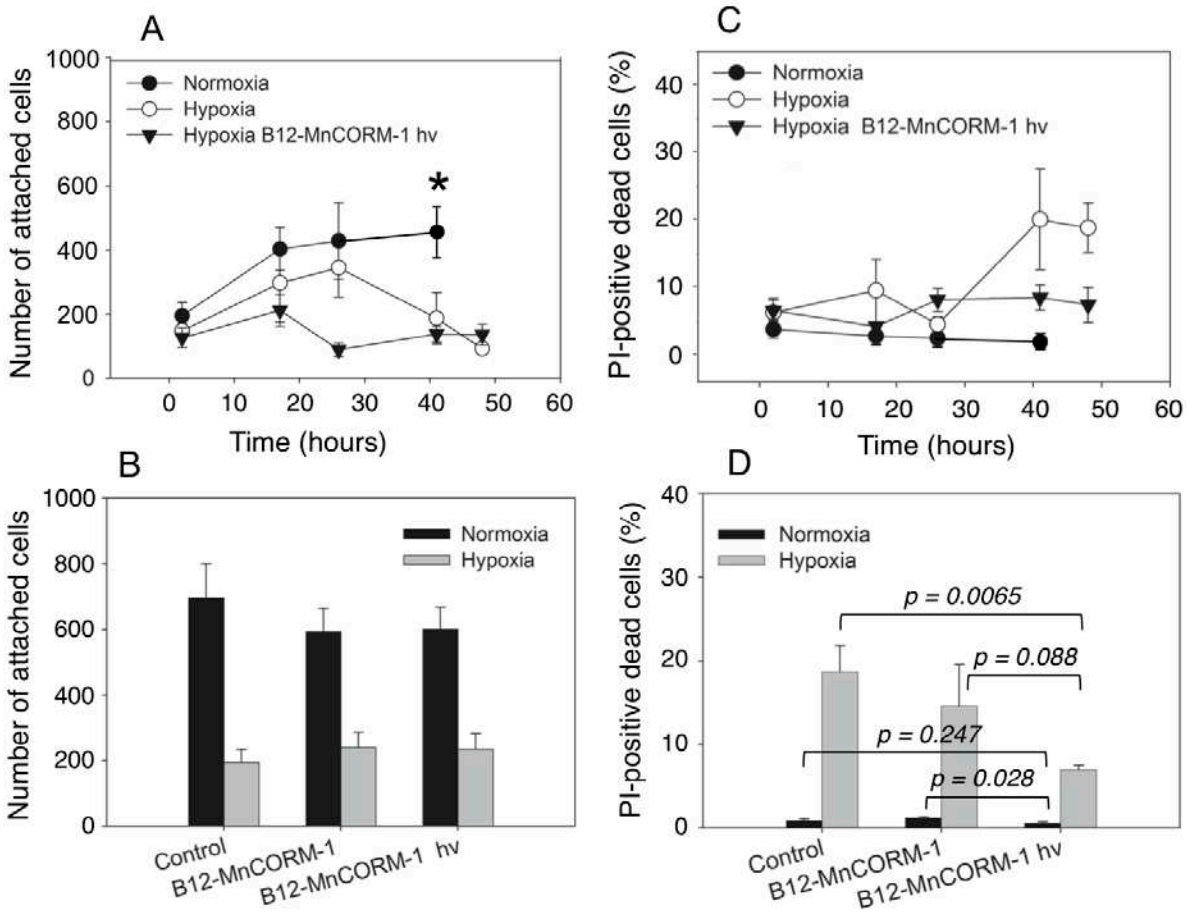

Figure 6. Effects of B_{12}-MnCORM-**1** on fibroblast cell cultures under different conditions. Normoxia: 5 mM glucose, 10% fetal bovine serum (FBS), pH 7.4 and 37ºC. Hypoxia: 0.2% O_2, 5% CO_2 and 94.8% N_2, pH 7.4 and 37ºC, no glucose, no FBS. B_{12}-MnCORM-**1** (30 µM) was added in the dark and activated by xenon lamp for 15 min when required. Time course of total number of cells attached to the substratum (A) and relative amount of dead cells (C) under conditions as indicated after staining with Hoechst-33342 and propidium iodide (PI). Number of attached cells (B) and percentage of dead cells (D) treated with inactive B_{12}-MnCORM-**1** and with light activated B_{12}-MnCORM-1 at 48 hours under normoxic or hypoxic conditions as indicated. Numbers of cells are total counts in 4 x 0.5 mm^2 of pre-determined microscope areas per culture dish (see Experimental Section). Experiments in (A and C) represent different series than in (B and D), but in all cases the number of independent experiments is 5. For further explanations see text. Data are means ± SEM. One-way ANOVA

with post-test Bonferroni correction (A and C) or non-paired Student's t-test (B and D) was used for assessment of significance. Asterisk in (A) at 41 hours of normoxia denotes t-values in comparison to both lower curves corresponding to $p<0.01$. Differences between normoxic and hypoxic conditions in (B) all have $p<0.01$.

Comparison of the same parameters between treatment with non-activated B_{12}-MnCORM-**1** and with light-activated B_{12}-MnCORM-**1** is shown in figure 6B and 6D for cultures after 48 hours under normoxic or hypoxic conditions. In this experimental series the normoxic and hypoxic control values of attached cells reached near 700 and 200, respectively (figure 6B). Addition of non-activated or light-activated B_{12}-MnCORM-**1** did not significantly change either of the attached cell number values. Of note, B_{12}-MnCORM-**1** only slightly reduced the attached cell number from ~700 close to ~600 under normoxia, while under hypoxia the cell numbers remained at ~240 both with non-activated as well as with light-activated B_{12}-MnCORM-**1**. Turning to the fractions of PI-positive dead cells still attaching to the substratum, light-activation of B_{12}-MnCORM-**1** significantly reduced the number of dead cells under normoxia when compared to the cultures with non-activated B_{12}-MnCORM-**1** ($p = 0.028$). Under hypoxic conditions there was a trend towards the same outcome with $p = 0.088$. However, a significant reduction of dead cells by activated B_{12}-MnCORM-**1** was also observed in comparison to hypoxia alone ($p = 0.0065$). Generally, the number of dead cells was below 5% under all conditions of normoxia (figure 6C and 6D). Taken together, activated B_{12}-MnCORM-**1** protected fibroblasts in culture from dying when the cells were under severe stress induced by hypoxia and metabolic depletion.

The fibroblasts in culture that settled to the bottom of the dish, developed a dense actin stress

fiber network, which supposedly attaches to the substratum via focal adhesion plaques involving complexes with over half a dozen proteins, including integrin, talin, paxilin, vinculin, alpha-actinin, fokal adhesion kinase and others.[50, 51] In addition, the stress fibers comprise smooth muscle alpha-actin and non-muscle myosin. The cytoskeletal development when fibroblasts attach to the substratum is considered to represent a differentiation step transforming fibroblasts to contractile myofibroblasts. Such actin stress fibers are virtually absent in the detached cells prone to death. Thus the occurrence of stress fibers may be taken as marker for cell attachment to the culture dish.

Phalloidin binds to filamentous F-actin and prevents its depolymerisation. Phalloidin conjugated with green Alexa Fluor® 488 (0.1 μM final concentration) was used to visualize the F-actin cytoskeleton in combination with nuclear staining with blue Hoechst-33342. Prior to staining cell cultures kept for 48 hours were washed twice with PBS, fixed with 4% paraformaldehyde and permeabilised with 0.2% Triton X-100 (figure 7). Under normoxia the dense and confluent cell culture exhibited an intensive green cytoskeletal staining (figure 7A). Under hypoxia either with or without non-activated B_{12}-MnCORM-**1** cells were fewer and exhibited an altered morphology (figure 7B and 7C). In both cases the cells were considerably larger than under normoxia. This may be no surprise, since in the normoxic confluent culture cell-cell contacts inhibited individual cell growth, while the fewer cells in hypoxia without such contacts were not inhibited and may have further grown, in fact, they hypertrophied. Moreover, many cells displayed rhomboid and triangular shapes with intense actin staining along the edges. In addition a number of cells exhibited long spindle-like extensions. Taken together, the cellular appearance in figure 7B and 7C left the impression as if the cells under hypoxia were in the process of retracting from their original position on the substratum and thus progressing towards cell death. In contrast, treatment with light-activated B_{12}-

MnCORM-**1** significantly reduced cell death under the harsh conditions of hypoxia and metabolic depletion (neither glucose nor FBS) (figure 7D). In this particular culture, cell size and density was almost comparable to that under normoxia (figure 7A) while the actin cytoskeleton was considerably less prominent under hypoxia with activated B_{12}-MnCORM-**1**. The actin cytoskeleton was somewhat variably expressed in cells of different sectional regions, more strongly in the central parts and less so in the peripheral regions. Why light-activated B_{12}-MnCORM-**1**, beside its beneficial life saving effect, on average reduced cell proliferation and attachment to the substratum (figure 6A) is presently unknown and requires further investigation.

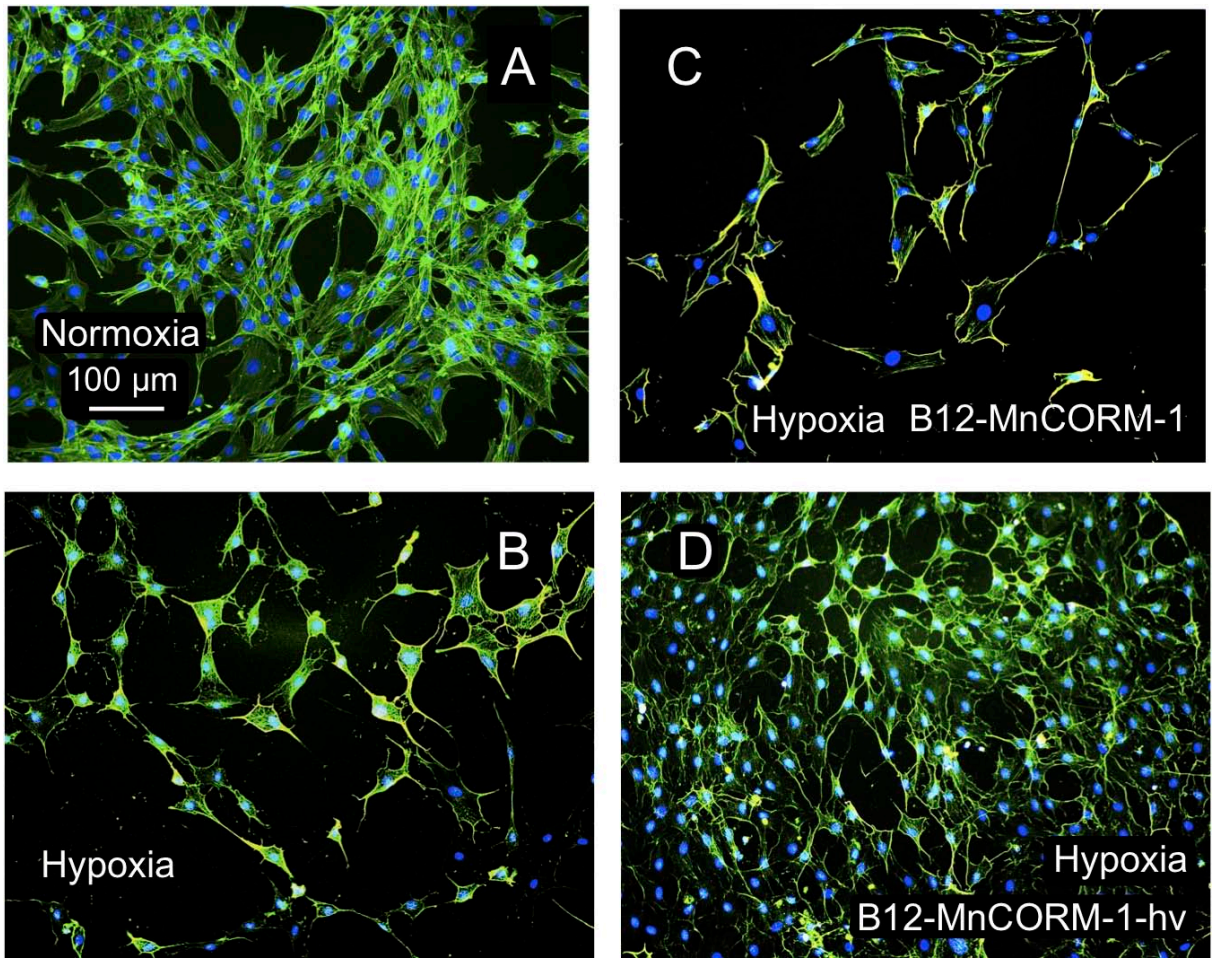

Figure 7. Representative histochemical staining of fibroblasts after 48 hours in culture under normoxia (A), hypoxia (B), treated with non-activated B_{12}-MnCORM-**1** (C) and with light-activated B_{12}-MnCORM-**1** (D). Staining of actin stress fibers in green with Alexa Fluor® 488 phalloidin and of nuclei with Hoechst-33342 in blue. Scale bar of 100 µm (A) is also valid for (B, C and D). For detailed description see text.

Conclusions

In conclusion, we have presented a novel B_{12}-conjugated photo-activated CO-releasing molecule appended on the ribose sugar moiety of the vitamin. Live 3T3 fibroblast cellular uptake of the molecule, investigated via synchrotron FTIR spectromicroscopy measurements, revealed that B_{12}-MnCORM-**1** was actively transported and internalized in 3T3 fibroblasts. The intracelluar photo-induced CO release of B_{12}-MnCORM-**1** could then be initiated with light of frequency in the visible region of the spectrum. The potential pharmacological value of the molecule was demonstrated by its cytoprotective effect on a cell culture model of 3T3 fribroblasts. The fibroblast cell culture system presented a sensitive model to test cytoprotective properties of CO-releasing transition metal complexes such as MnCORM coupled to cyanocobalamin (B_{12}). In the case of B_{12}-MnCORM-**1** the cobalamin moiety helps the compound to accumulate in the fibroblasts via a complex transport machinery that operates against a concentration gradient. Once inside the cell, B_{12}-MnCORM-**1** can be activated by light photolysis to release CO. We have shown that light-activated B_{12}-MnCORM-**1** protects fibroblasts from death under conditions of hypoxia and metabolic depletion. Without light activation B_{12}-MnCORM-**1** has no protective properties. The strenuous cell culture conditions at insufficient supply of oxygen and nutrients may mimic

comparable situations during hypoperfusion of oxygen-sensitive tissues such as the heart or brain in vivo.

Acknowledgements

FZ acknowledges the Swiss National Science Foundation (Ambizione Grant# PZ00P2_121989) for financial support. LQ acknowledges internal funding form the Swiss Light Source and the Paul Scherrer Institut. The authors are grateful to Elise Normand for writing and supporting the software MIDAS for 2D-COS and to Dr. Marc Creus (University of Basel) for helpful discussion.

Experimental Section

Chemicals and solvents for synthesis were purchased from standard sources. All synthesis were performed under an inert N_2 atmosphere unless otherwise noted. Elemental analyses (EA) were performed on a Leco CHNS-932 elemental analyzer. Atomic absorption measurements were carried out using a Varian AA 240FS fast sequential atomic absorption spectrometer. Solid state IR spectra were recorded in a PerkinElmer Spectrum BX FT-IR spectrometer. Liquid IR spectra were measured with an *in situ* deep IR probe of a Mettler Toledo ReactIR iC10 system. UV/Vis spectra were taken on a Perkin Elmer Cary 50 spectrometer with a Peltier thermostat. Mass spectra were recorded in the positive mode on an Esquire HCT from Bruker (Bremen, Germany) with electrospray ionization (ESI). High-resolution electrospray mass spectra were recorded on a Bruker maXis QTOF-MS instrument (Bruker Daltonics GmbH, Bremen, Germany). The samples were dissolved in a 1:1 mixture of MeOH and 0.1% formic acid and analyzed via continuous flow injection at 30 µL/min. The mass spectrometer was operated in positive ion mode with a capillary voltage of 4 kV, an endplate offset of –500 V, nebulizer pressure of 5.8

psig, and a drying gas flow rate of 4 L/min at 180°C. The instrument was calibrated with a sodium formate solution (500µl H_2O : 500µl iPrOH : 20ul HCOOH : 20µl 0.1M $NaOH_{aq}$). The resolution was optimized at 30'000 FWHM in the active focus mode. The accuracy was better than 2 ppm in a mass range between m/z 118 and 2000. All solvent used were purchased in best LC-MS qualities.

Analytical HPLC method.

Instrument: MERCK HITACHI LaChrom with a D-7000 interface coupled with a Diode Array detector L-7455 and a pump L-7100 system. Column: Macherey-Nagel, EC250/3 Nucleosil 100-5 C18. Flow rate 0.5 mL/min. Absorbance monitored at 250 nm. Solutions: A: 0.1% trifluoroacetic acid in water; B: methanol. Chromatographic method: 0-5 min: isocratic flow of 75% A-25% B; 5-40 min: linear gradient to 100% B.

Atomic Absorption Spectrometry.

The 3T3 cells were plated in fifteen 6cmó r -dishes and grown in DMEM medium supplemented with 10% foetal calve serum and penicilin-streptomycin mixture to 70% confluence. Six of them were then treated with 100 µM B_{12}-MnCORM-**1** dissolved in DMEM whereas the other six plate ere used as control. Treatment of 3T3cells with B_{12}-MnCORM-**1** in the absence of light lasted 6 h. Thereafter the medium was collected for analysis and the cells were washed three times with PBS. After the removal of PBS, three Petri-dishes per condition were wet-burned with concentrated trace metal-free HNO_3 (300 µl total volume) and the retained total intracellular B_{12}-MnCORM-**1** content was measured using atomic absorption spectrophotometry. The other three samples per condition were placed on ice and treated for 10 minutes with a cell lysis buffer containing 0.27 M sucrose, 2 mM EDTA (pH 8.0), 0.1% NP-40, in 0.6 M KCl, 150 mM NaCl, 150 mM HEPES (pH 7.5). This buffer perforated plasma membranes and released cytosolic

components leaving nuclear membranes unaffected. This protocol was successfully used for isolation of nuclear fraction in various cell lines and primary cell cultures.[52] The lysis buffer containing cytosolic proteins was then removed and the remanining perforated cells washed with PBC and burned with HNO_3. Cells in the remaining three Petri dishes were washed with PBS and lysed in 200 µl 0.1 M NaOH and used for protein detection using Biorad protein assay. Manganese content was assessed in control and CORM-treated cells and in the corresponding nuclear fractions and the values normalised per amount of protein (180 ±16 mg per Petri-dish).

Computational Details.

Geometry optimizations, as well as frequency calculations for all molecules, were performed at the Density Functional level of theory with the Gaussian03 program package[53] using the hybrid B3LYP functional[54] in conjunction with the LanL2DZ basis set. [55-57] Pure basis functions (5d, 7f) were used in all calculations. Geometries were fully optimized without symmetry restrictions. The nature of the stationary points was checked by computing vibrational frequencies in order to verify true minima. The molecular structures of B_{12}-MnCORM-**1** and B_{12}-MnCORM-**1a** were optimized by the two-layer ONIOM method[58, 59] using the DFT method B3LYP/LanL2DZ for the high layer and the molecular mechanics method UFF for the low layer (see description of the layers in SI).[60]

Synthesis of B_{12}-tacd (1).

Cyanocobalamin (135 mg, 0.1 mmol) was dissolved in 10 ml of dry DMSO. A total of 24.6 mg of carbonylditriazole (CDT) (0.15 mmol) was added. After stirring at RT overnight, 200 mg of tacd (where tacd = 1,4,8,11-tetraazacyclotetradecane, 1 mmol) were added. The mixture was stirred for 24h and then dried under vacuum. The resulting red

powder was purified by preparative HPLC to yield 120mg (75.8%) of **1**. Analytical data for **1**: HPLC: retention time 7.9 min. ESI-MS analysis (positive mode) gave peaks at *m/z* = 1582.2 $[M^+]$ and 791.8 $[M+H^+]^{2+}$. ^{13}C NMR, 100 MHz (D_2O, δ ppm): 18.0; 18.2; 18.6; 19.6; 21.9 (3C); 22.0; 22.2; 22.7; 28.0; 28.8 (1-2C); 30.8; 34.1; 34.2; 34.6; 35.0; 35.5; 37.5; 37.7 ; 41.8; 45.6; 45.7; 45.9 (3C); 48.1(1-3C); 49.4(2C); 50.1; 50.9; 54.2; 56.6; 58.5; 59.1; 62.0; 65.8; 71.4; 75.5; 75.8; 75.9; 77.7; 81.9; 87.9; 89.7; 97.8; 106.9; 110.3; 114.1; 119.4; 132.8; 135.8; 137.9; 139.5; 144.6; 158.8 168.1; 168.8; 176.4; 177.5; 177.9; 178.5; 178.0; 179.7; 180.0; 180.7; 181.0; 181.7; 182.8; I.r. (solid state, KBr, cm^{-1}): $\nu_{C\equiv N}$ 2134.

Synthesis of B_{12}-[(tacd)$Mn^I(CO)_3$](CF_3CO_2) (B_{12}-MnCORM-1).

A total of 115 mg of **1** (0.074 mmol) was dissolved in 4 ml of dry MeOH. To the solution 89 mg of $[Mn^IBr(CO)_5]$ (0.3 mmol, 4.5 eq) and 100 µl of triethylamine (TEA) were added. After 24h of stirring at RT, the solution was dried under vacuum. The resulting red powder was purified by preparative HPLC to yield 23mg (18.1%) of the desired product. Analytical data for B_{12}-MnCORM-**1**: HPLC: retention time 21.9 min. ESI-MS analysis (positive mode) gave peaks at *m/z* = 1720.6 $[M^+]$ and 860.7 $[M+H^+]^{2+}$. ^{13}C NMR, 100 MHz (D_2O, δ ppm): 18.0 (2C); 18.5; 19.3; 21.5 (3C); 21.9; 22.1 (2C); 28.5 (2C); 30.5; 33.8; 34.2 (2C); 34.9 (2C); 37.5 (2C); 41.5; 45.3; 45.5 (3C); 48.0; 49.1 (4C); 50.1 (3C); 50.8 (2C); 54.2; 56.0; 58.2; 58.8; 62.0; 63.0; 71.4; 75.5 (2C); 77.5; 84.6; 87.9; 89.5; 97.5; 107.0, 110.3; 114.0; 119.1; 132.7; 135.8; 137.8; 139.5; 144.3; 168.5 (2C); 176.4; 177.7 (2C); 178.6 (2C); 179.8, 180.0, 180.7 (2C); 181.0; 182.8; 195.1 (3C). I.r. (solid state, KBr, cm^{-1}): $\nu_{C\equiv O}$ 2026, 1922; $\nu_{C\equiv N}$ 2134. In this reaction a second minor product (B_{12}-MnCORM-**1a**, *vide infra*) was also identified and isolated. Yield 3.8mg (3 %). Analytical data for B_{12}-MnCORM-**1a**: HPLC: retention time 23.9 min. ESI-MS analysis (positive mode) gave peaks at *m/z* = 1720.6 $[M^+]$ and 860.7 $[M+H^+]^{2+}$. I.r. (solid state, KBr, cm^{-1}):

$\nu_{C\equiv O}$ 2026, 1922; $\nu_{C\equiv N}$ 2134.

Synthesis of *fac*-[(tacd)$Mn^{I}(CO)_3$]Br (2).

A total of 418 mg of $Mn(CO)_5Br$ (1.5 mmol) were dissolved in 7 ml of dry DMF. To the solution 300 mg of tacd (1.5 mmol, 1 eq) were added. After 24h of stirring at RT, the resulting yellow solution was dried under vacuum. The residue was then purified by preparative HPLC to yield 293mg (57%) of **2**. Analytical data for **2**. Anal. Calc. for $C_{13}H_{24}Br_1N_4O_3Mn$ (419.2): C 37.25%, H 5.77%, N 13.37%. Found: C 37.58%, H 6.01%, N 13.45%. HPLC: retention time 19.8 min. ESI-MS analysis (positive mode) gave a single peak at *m/z* = 339.2 [M^+]. I.r. (solid state, KBr, cm^{-1}): $\nu_{C\equiv O}$ 2031, 1922.

Fibroblast Cell Culture for FTIR Spectromicroscopy Measurements.

NIH 3T3 Swiss Albino Mouse Fibroblast cells (ECACC Catalogue Number 85022108) were cultured directly on CaF_2 windows (Crystran, Poole, UK) in Dulbecco's Modified Eagle Medium (DMEM) containing 5 mM glucose and 10% fetal bovine serum (FBS). Cells were grown for 16 to 24 hours, until the desired degree of coverage was obtained (about 20% - 30%). The cell-coated window was transferred to a custom-built solution sample holder for FTIR microscopy, as previously described.[38] All cell culture materials were purchased from Invitrogen (Invitrogen, Life Technologies, Paisley, UK).

Fibroblast Cell Treatment.

Cell treatment with the CORM was performed under dim light. Additon of B_{12}-MnCORM-**1** was performed by first removing bulk DMEM medium and covering the window with a DMEM solution of B_{12}-MnCORM-**1** of 0.1-1 mM. The sample holder was

then enclosed, kept at 37°C and used for FTIR spectromicroscopy measurements.

FTIR Spectromicroscopy Measurements.

FTIR Spectromicroscopy experiments were performed at beamline X01DC of the Swiss Light Source, comprising a Bruker Vertex 70v interferometer (Bruker Optics) and a Bruker Hyperion 3000 microscope. For these measurements, a KBr-supported Ge-multilayer beamsplitter was used together with a liquid nitrogen-cooled MCT detector. The interferometer was scanned with an acquisition rate of 40 kHz to 4 cm-1 resolution. Measurements were performed in transmission. 250 scans were collected for each measurements, with a 60 s interval between measurements. Single channel spectra were obtained by performing a Fourier Transform of the interferogram after apodization with a Blackman-Harris 3-Term function, using a zero-filling factor of 2 and a Mertz phase correction.

In a single cell photolysis experiment, an isolated cell was selected under the IR microscope using weak illumination. The confocal apertures where closed to limit the field probed by the IR light to a rectangle corresponding to the body of the cell. In the case of measurements on 3T3 fibroblasts, this selection excludes the filipodia. The cell was monitored for a few minutes by measuring sequential FTIR spectra in dim light. During this period, uptake of B_{12}-MnCORM-**1** was followed by observing the increase of absorption bands due to the CO ligands of B_{12}-MnCORM-**1** at 2027 cm^{-1} and 1931 cm^{-1}. After 60 min the cell was irradiated with the full spectrum from the 100W halogen lamp of the microscope illuminator and photolysis of the CORM was followed by the decrease of the same bands.

FTIR Mapping Measurements.

The distribution of IR absorption bands was recorded by mapping the sample over a rectangular grid pattern. For the higest resolution maps, confocal blades were set to a square aperture of 5x5 μm^2 and point spacing was set at 2.5 μm. Using a 36x objective with 0.5 NA, these conditions give a theroetical spatial resolution close to the diffraction limit at the walength of absorption of CO ligands. For low resolution maps, confocal blades were set to an aperture of 10x10 μm^2 and point spacing was set at 5 or10 μm.

Data Analysis.

FTIR data analysis and assembly of IR maps was performed using the software package OPUS 6.5 (Bruker Optics). Spectral plots were constructed using Origin 8.0 (Originlab, Northampton, MA,USA).

Fibroblast Cell Culture for Biological Tests.

After 5-8 passages 3T3 cells were cultured in DMEM supplemented with 5 mM glucose and 10% FBS plus penicillin-streptomycin at pH 7.4. About one million cells were plated per Petri dish of 4.5 cm^2 area and kept proliferating to near confluence at 37 ºC in the presence of 95% air and 5% CO2 as described earlier.[7] Thereafter, the medium was exchanged in order to establish the following experimental conditions.

Normoxic control cultures containing 5 mM glucose and 10% FBS were kept at pH 7.4 with phosphate buffered saline (PBS). Metabolically depleted cells were cultured in DMEM without glucose nor FBS in an incubator with a gas phase containing 0.2% O_2, 5% CO_2 and 94.8% N_2 (hypoxia) at 37 ºC and pH 7.4. Stock solution of B_{12}-MnCORM-**1** was taken up in PBS and added under dim light to give a final concentration of 30 μM to both normoxic and

metabolically depleted cultures as indicated in figure 6. Ten minutes after administration of B_{12}-MnCORM-**1** half of the cultures were exposed to light (xenon lamp at a distance of 10 cm) for 15 min and the other half kept in darkness. The light-exposed cultures were subsequently kept under bench light during the whole experiment whereas those in the dark remained protected from light for the rest of the incubation time.

Responses of cells to metabolic depletion were followed from 2 till 48 hours as reflected in the proportion of live and dead cells attached to the bottom of the culture dishes. Cell cultures were stained for 10 min with a mixture of 10 µg/ml Hoechst-33342 and 10 µg/ml propidium iodide (PI) (Invitrogen, Molecular Probes). Hoechst-33342 (excitation and emission maxima 360 and 450 nm, respectively) is membrane-permeable and stains the nuclei of all cells by binding to double-stranded nuclear DNA. Membrane-impermeable PI (excitation and emission maxima 555 and 620 nm, respectively) intercalates with DNA and RNA and is commonly used for identifying dead cells with ruptured plasma membrane. Fluorescent staining was recorded using the Axiovert 200-M fluorescent microscope and analyzed using MCID™ image analysis software.[7] Staining with Alexa Fluor® 488 phalloidin (0.1 µM final concentration) was used to visualize the F-actin cytoskeleton. This double staining was performed after twice washing with PBS, fixation with 4% paraformaldehyde, and permeabilisation with 0.2% Triton X-100.

In each culture dish cells were counted in 5 predetermined areas of 0.5 mm^2, totalling 2.5 mm^2 per dish. After checking for normal distribution statistical analysis by one-way ANOVA was performed by non-paired Student's t-test using GraphPad Instat (GraphPad Inc. La Jolla, CA). Data are expressed as means (5 independent experiments each) ± SEM and considered significant when two-tailed $p < 0.05$.

References

1. Wu, L. Y.; Wang, R. Carbon monoxide: Endogenous production, physiological functions, and pharmacological applications. *Pharmacol. Rev.* **2005,** 57, 585-630.
2. Motterlini, R.; Otterbein, L. E. The therapeutic potential of carbon monoxide. *Nat. Rev. Drug Discov.* **2010,** 9, 728-742.
3. Mann, B. E. Carbon Monoxide: An Essential Signalling Molecule. *Top. Organomet. Chem.* **2010,** 32, 247-285.
4. Vummaleti, S. V. C.; Branduardi, D.; Masetti, M.; De Vivo, M.; Motterlini, R.; Cavalli, A. Theoretical Insights into the Mechanism of Carbon Monoxide (CO) Release from CO-Releasing Molecules. *Chem. Eur. J.* **2012,** 18, 9267-9275.
5. Crook, S. H.; Mann, B. E.; Meijer, A. J. H. M.; Adams, H.; Sawle, P.; Scapens, D.; Motterlini, R. [Mn(CO)(4){S2CNMe(CH2CO2H)}], a new water-soluble CO-releasing molecule. *Dalton Trans.* **2011,** 40, 4230-4235.
6. Hewison, L.; Crook, S. H.; Mann, B. E.; Meijer, A. J. H. M.; Adams, H.; Sawle, P.; Motterlini, R. A. New Types of CO-Releasing Molecules (CO-RMs), Based on Iron Dithiocarbamate Complexes and [Fe(CO)(3)I(S2COEt)]. *Organometallics* **2012,** 31, 5823-5834.
7. Zobi, F.; Blacque, O.; Jacobs, R. A.; Schaub, M. C.; Bogdanova, A. Y. 17 e(-) rhenium dicarbonyl CO-releasing molecules on a cobalamin scaffold for biological application. *Dalton Trans.* **2012,** 41, 370-378.
8. Atkin, A. J.; Fairlamb, I. J. S.; Ward, J. S.; Lynam, J. M. CO Release from Norbornadiene Iron(0) Tricarbonyl Complexes: Importance of Ligand Dissociation. *Organometallics* **2012,** 31, 5894–5902.
9. Zhang, W. Q.; Atkin, A. J.; Fairlamb, I. J. S.; Whitwood, A. C.; Lynam, J. M. Synthesis and Reactivity of Molybdenum Complexes Containing Functionalized Alkynyl Ligands: A Photochemically Activated CO-Releasing Molecule (PhotoCO-RM). *Organometallics* **2011,** 30, 4643-4654.
10. Zhang, W. Q.; Atkin, A. J.; Thatcher, R. J.; Whitwood, A. C.; Fairlamb, I. J. S.; Lynam, J. M. Diversity and design of metal-based carbon monoxide-releasing molecules (CO-RMs) in aqueous systems: revealing the essential trends. *Dalton Trans.* **2009**, 4351-4358.
11. Atkin, A. J.; Williams, S.; Sawle, P.; Motterlini, R.; Lynam, J. M.; Fairlamb, I. J. S. mu(2)-Alkyne dicobalt(0)hexacarbonyl complexes as carbon monoxide-releasing molecules (CO-RMs): probing the release mechanism. *Dalton Trans.* **2009**, 3653-3656.
12. Fairlamb, I. J. S.; Lynam, J. M.; Moulton, B. E.; Taylor, I. E.; Duhme-Klair, A. K.; Sawle, P.; Motterlini, R. h(1)-2-pyrone metal carbonyl complexes as CO-releasing molecules (CO-RMs): A delicate balance between stability and CO liberation. *Dalton Trans.* **2007**, 3603-3605.
13. Romanski, S.; Kraus, B.; Guttentag, M.; Schlundt, W.; Rucker, H.; Adler, A.; Neudorfl, J.-M.; Alberto, R.; Amslinger, S.; Schmalz, H.-G. Acyloxybutadiene tricarbonyl iron complexes as enzyme-triggered CO-releasing molecules (ET-CORMs): a structure-activity relationship study. *Dalton Trans.* **2012,** Advance Article.
14. Romanski, S.; Kraus, B.; Schatzschneider, U.; Neudorfl, J. M.; Amslinger, S.; Schmalz, H. G. Acyloxybutadiene-Iron Tricarbonyl Complexes as Enzyme-Triggered CO-Releasing Molecules (ET-CORMs). *Angew. Chem. Int. Ed.* **2011,** 50, 2392-2396.
15. Rimmer, R. D.; Pierri, A. E.; Ford, P. C. Photochemically activated carbon monoxide release for biological targets. Toward developing air-stable photoCORMs labilized by visible light. *Coord. Chem. Rev.* **2012,** 256, 1509-1519.
16. Rimmer, R. D.; Richter, H.; Ford, P. C. A Photochemical Precursor for Carbon Monoxide Release in Aerated Aqueous Media. *Inorg. Chem.* **2010,** 49, 1180-1185.
17. Schatzschneider, U. PhotoCORMs: Light-triggered release of carbon monoxide from the coordination sphere of transition metal complexes for biological applications. *Inorg. Chim. Acta* **2011,** 374, 19-23.

18. Desmard, M.; Davidge, K. S.; Bouvet, O.; Morin, D.; Roux, D.; Foresti, R.; Ricard, J. D.; Denamur, E.; Poole, R. K.; Montravers, P.; Motterlini, R.; Boczkowski, J. A carbon monoxide-releasing molecule (CORM-3) exerts bactericidal activity against Pseudomonas aeruginosa and improves survival in an animal model of bacteraemia. *Faseb J.* **2009,** 23, 1023-1031.
19. McLean, S.; Mann, B. E.; Poole, R. K. Sulfite species enhance carbon monoxide release from CO-releasing molecules: Implications for the deoxymyoglobin assay of activity. *Anal. Biochem.* **2012,** 427, 36-40.
20. Smith, H.; Mann, B. E.; Motterlini, R.; Poole, R. K. The Carbon Monoxide-releasing Molecule, CORM-3 (Ru(CO)(3)Cl(Glycinate)), Targets Respiration and Oxidases in Campylobacter jejuni, Generating Hydrogen Peroxide. *Iubmb Life* **2011,** 63, 363-371.
21. Davidge, K. S.; Sanguinetti, G.; Yee, C. H.; Cox, A. G.; McLeod, C. W.; Monk, C. E.; Mann, B. E.; Motterlini, R.; Poole, R. K. Carbon Monoxide-releasing Antibacterial Molecules Target Respiration and Global Transcriptional Regulators. *J. Biol. Chem.* **2009,** 284, 4516-4524.
22. Wilson, J. L.; Jesse, H. E.; Hughes, B. M.; Lund, V.; Naylor, K.; Davidge, K. S.; Cook, G. M.; Mann, B. E.; Poole, R. K. Ru(CO)3Cl(glycinate) (CORM-3): a CO-releasing molecule with broad-spectrum antimicrobial and photosensitive activities against respiration and cation transport in Escherichia coli. *Antioxid Redox Signal* **2013**, in press.
23. Zobi, F.; Blacque, O. Reactivity of 17 e- Complex [ReII(Br)4(CO)(2)](2-) with Bridging Aromatic Ligands. Characterization and CO-Releasing Properties. *Dalton Trans.* **2011,** 40, 4994-5001.
24. Zobi, F.; Degonda, A. CO-releasing properties of cis-trans-[Re-II(CO)(2)Br2L2](n) complexes. *Nucl. Med. Biol.* **2010,** 37, 712-712.
25. Zobi, F.; Degonda, A.; Schaub, M. C.; Bogdanova, A. Y. CO Releasing Properties and Cytoprotective Effect of cis-trans- [Re-II(CO)(2)Br2L2](n) Complexes. *Inorg. Chem.* **2010,** 49, 7313-7322.
26. Moreira, E. S.; Brasch, N. E.; Yun, J. Vitamin B-12 protects against superoxide-induced cell injury in human aortic endothelial cells. *Free Rad. Biol. Med.* **2011,** 51, 876-883.
27. Hygum, K.; Lildballe, D. L.; Greibe, E. H.; Morkbak, A. L.; Poulsen, S. S.; Sorensen, B. S.; Petersen, T. E.; Nexo, E. Mouse Transcobalamin Has Features Resembling both Human Transcobalamin and Haptocorrin. *Plos One* **2011,** 6, e20638.
28. Wuerges, J.; Garau, G.; Geremia, S.; Fedosov, S. N.; Petersen, T. E.; Randaccio, L. Structural basis for mammalian vitamin B-12 transport by transcobalamin. *Proc. Natl. Acad. Sci. USA* **2006,** 103, 4386-4391.
29. Vortherms, A. R.; Kahkoska, A. R.; Rabideau, A. E.; Zubieta, J.; Andersen, L. L.; Madsen, M.; Doyle, R. P. A water soluble vitamin B-12-Re(I) fluorescent conjugate for cell uptake screens: use in the confirmation of cubilin in the lung cancer line A549. *Chem. Commun.* **2011,** 47, 9792-9794.
30. Kunze, S.; Zobi, T.; Kurz, P.; Spingler, B.; Alberto, R. Vitamin B12 as a ligand for technetium and rhenium complexes. *Angew. Chem. Int. Ed.* **2004,** 43, 5025-5029.
31. Mundwiler, S.; Spingler, B.; Kurz, P.; Kunze, S.; Alberto, R. Cyanide-bridged vitamin B-12-cisplatin conjugates. *Chem. Eur. J.* **2005,** 11, 4089-4095.
32. Ruiz-Sanchez, P.; Mundwiler, S.; Medina-Molner, A.; Spingler, B.; Alberto, R. Iodination of cisplatin adduct of Vitamin B-12 [{B-12}-CN-{cis-PtCl(NH3)(2)}](+). *J. Organomet. Chem.* **2007,** 692, 1358-1362.
33. Zobi, F.; Kromer, L.; Spingler, B.; Alberto, R. Synthesis and Reactivity of the 17 e(-) Complex [(ReBr4)-Br-II(CO)(2)](2-): A Convenient Entry into Rhenium(II) Chemistry. *Inorg. Chem.* **2009,** 48, 8965-8970.
34. Günzler, H.; Gremlich, H.-U. *IR Spectroscopy*. Wiley-VCH: 2002.
35. Miller, L. M.; Carr, G. L.; Williams, G. P.; Chance, M. R. Synchrotron infrared microspectroscopy as a means of studying chemical composition at a cellular level. *Biophys. J.* **1997,** 72, TU445-TU445.

36. Matthaeus, C.; Bird, B.; Miljkovic, M.; Chernenko, T.; Romeo, M.; Diem, M. Infrared and Raman Microscopy in Cell Biology. In *Biophysical Tools for Biologists, Vol 2: in Vivo Techniques*, Correia, J. J.; III, H. W. D., Eds. Elsevier: 2008; Vol. 89, pp pp. 275-308.
37. Carr, G. L. Resolution limits for infrared microspectroscopy explored with synchrotron radiation. *Rev. Sci. Instrum.* **2001,** 72, 1613-1619.
38. Quaroni, L.; Zlateva, T. Infrared spectromicroscopy of biochemistry in functional single cells. *Analyst* **2011,** 136, 3219-3232.
39. Holman, H. Y. N.; Bechtel, H. A.; Hao, Z.; Martin, M. C. Synchrotron IR Spectromicroscopy: Chemistry of Living Cells. *Anal. Chem.* **2011,** 82, 8757-8765.
40. Quaroni, L.; Zlateva, T.; Normand, E. Detection of Weak Absorption Changes from Molecular Events in Time-Resolved FT-IR Spectromicroscopy Measurements of Single Functional Cells. *Anal. Chem.* **2011,** 83, 7371-7380.
41. Noda, I. Generalized two-dimensional correlation spectroscopy. *Front. Mol. Spectrosc.* **2009**, 367-381.
42. Massaro, S.; Zlateva, T.; Torre, V.; Quaroni, L. Detection of molecular processes in the intact retina by ATR-FTIR spectromicroscopy. *Anal. Bioanal. Chem.* **2008,** 390, 317-322.
43. Quaroni, L.; Normand, E. Two-Dimensional Correlation Spectroscopy Analysis for the Recovery of Weak Bands from Time-Resolved Infrared Spectra of Single Cells. In *Wirms 2009: 5th International Workshop on Infrared Microscopy and Spectroscopy with Accelerator Based Sources*, 2010; Vol. 1214, pp 66-68.
44. Ye, X. D.; Fels, D.; Tovmasyan, A.; Aird, K. M.; Dedeugd, C.; Allensworth, J. L.; Kos, I.; Park, W.; Spasojevic, I.; Devi, G. R.; Dewhirst, M. W.; Leong, K. W.; Batinic-Haberle, I. Cytotoxic effects of Mn(III) N-alkylpyridylporphyrins in the presence of cellular reductant ascorbate. *Free Radic. Res.* **2011,** 45, 1289-1306.
45. Woo, E. S.; Lazo, J. S. Nucleocytoplasmic functionality of metallothionein. *Cancer Res.* **1997,** 57, 4236-4241.
46. Meister, K.; Niesel, J.; Schatzschneider, U.; Metzler-Nolte, N.; Schmidt, D. A.; Havenith, M. Label-Free Imaging of Metal-Carbonyl Complexes in Live Cells by Raman Microspectroscopy. *Angew. Chem. Int. Ed.* **2010,** 49, 3310-3312.
47. Policar, C.; Waern, J. B.; Plamont, M. A.; Clede, S.; Mayet, C.; Prazeres, R.; Ortega, J. M.; Vessieres, A.; Dazzi, A. Subcellular IR Imaging of a Metal-Carbonyl Moiety Using Photothermally Induced Resonance. *Angew. Chem. Int. Ed.* **2011,** 50, 860-864.
48. Jamin, N.; Miller, L.; Moncuit, J.; Fridman, W.-H.; Dumas, P.; Teillaud, J.-L. Chemical heterogeneity in cell death: Combined synchrotron IR and fluorescence microscopy studies of single apoptotic and necrotic cells. *Biopolymers* **2003,** 72, 366-373.
49. Nielsen, M. J.; Rasmussen, M. R.; Andersen, C. B. F.; Nexo, E.; Moestrup, S. K. Vitamin B-12 transport from food to the body's cells-a sophisticated, multistep pathway. *Nat. Rev. Gastro. Hepat.* **2012,** 9, 345-354.
50. Vicente-Manzanares, M.; Ma, X. F.; Adelstein, R. S.; Horwitz, A. R. Non-muscle myosin II takes centre stage in cell adhesion and migration. *Nat. Rev. Mol. Cell Biol.* **2009,** 10, 778-790.
51. Hinz, B. The myofibroblast: Paradigm for a mechanically active cell. *J. Biomech.* **2010,** 43, 146-155.
52. Schmid-Brunclik, N.; Burgi-Taboada, C.; Antoniou, X.; Gassmann, M.; Ogunshola, O. O. Astrocyte responses to injury: VEGF simultaneously modulates cell death and proliferation. *Am. J. Physiol. Reg. Integr. Comp. Physiol.* **2008,** 295, R864-R873.
53. Iyengar, S. S.; Frisch, M. J. Effect of time-dependent basis functions and their superposition error on atom-centered density matrix propagation (ADMP): Connections to wavelet theory of multiresolution analysis. *J. Chem. Phys.* **2004,** 121, 5061-5070.
54. Becke, A. D. Density functional thermochemistry. III. The role of exact exchange *J. Chem. Phys.* **1993,** 98, 5648-5652.

55. Hay, P. J.; Wadt, W. R. Ab initio effective core potentials for molecular calculations. Potentials for the transition metal atoms Sc to Hg. *J. Chem. Phys.* **1985,** 82, 270-283.
56. Hay, P. J.; Wadt, W. R. Ab initio effective core potentials for molecular calculations. Potentials for K to Au including the outermost core orbitals *J. Chem. Phys.* **1985,** 82, 299-310.
57. Wadt, W. R.; Hay, P. J. Ab initio effective core potentials for molecular calculations. Potentials for main group elements Na to Bi *J. Chem. Phys.* **1985,** 82, 284-298.
58. Dapprich, S.; Komaromi, I.; Byun, K. S.; Morokuma, K.; Frisch, M. J. A new ONIOM implementation in Gaussian98. Part I. The calculation of energies, gradients, vibrational frequencies and electric field derivatives. *J. Mol. Struct. (Theochem)* **1999,** 462, 1-21.
59. Vreven, T.; Byun, K. S.; Komaromi, I.; Dapprich, S.; Montgomery, J. A.; Morokuma, K.; Frisch, M. J. Combining quantum mechanics methods with molecular mechanics methods in ONIOM. *J. Chem. Theory Comput.* **2006,** 2, 815-826.
60. Rappe, A. K.; Casewit, C. J.; Colwell, K. S.; Goddard, W. A.; Skiff, W. M. Uff, a Full Periodic-Table Force-Field for Molecular Mechanics and Molecular-Dynamics Simulations. *J. Am. Chem. Soc.* **1992,** 114, 10024-10035.

Table of Contents graphic